AIAA Guidance Naviation & Control Conference, August 2007, Hilton Head, South Carolina

Formation Flying Control in Highly Elliptical Orbits

A. Marcos * and L.F. Peñín †

Advanced Projects Division, Deimos Space S.L., Madrid, 28760, Spain

E. Di Sotto, ‡

Advanced Projects Division, Deimos Engeharia S.A., Lisbon, 1998-023, Portugal

R. Drai §

ESA-ESTEC, Noordwijk, 2200, The Netherlands

In this paper a satellite formation flying control design based on nonlinear dynamic inversion is presented. The formation consists of three satellites using a relative leader-follower control scheme flying a highly elliptical orbit around Earth. The resulting controller is subject to environment effects (J2), uncertainty, strong navigation errors and noise using a state-of-the-art formation flying engineering simulator. The results show that the resulting closed-loop can cope successfully with all the considered perturbations while satisfying performance & robustness design requirements throughout the experimental phase of orbit and that during perigee passages it performs reasonably well.

I. Introduction

The formation-flying (FF) concept has recently become popular in Space remote and long-term missions due to its advantages, capabilities and flexibility. Among other benefits, a multiple platform mission allows for: reduced size, complexity and cost of spacecrafts; Increased robustness, as functions are distributed along the formation spacecrafts; Increased instrument resolution; And, increased flexibility in mission scenarios.

Adequate implementation of the formation coordination and control scheme selected lies on the capability of the spacecrafts (SCs) within the formation to fulfil the functions allocated to them. These functions are typically implemented through dedicated equipment in the GNC chain. The better that each spacecraft is capable of achieving the individual objectives imposed by the coordination architecture, the better the formation will perform as a whole.

Within this FF-GNC chain, FF control can be defined as a set of more than one spacecraft whose dynamic states are coupled through a common control law. In particular, at least one member of the set must track a desired state relative to another member and the tracking control law must at least depend upon the state of this other member.

Similarly to the FF concept, highly elliptical orbits (HEO) are currently being evaluated for future scientific observation missions since they offer a sufficiently quiet environment for FF experimentation around apogee while increasing the experimentation time. The main drawback for HEO is that they undergo drastic gravity gradient effects around perigee representing a major FF-GNC design challenge (up to considering this orbit location unsuitable for multiple-SC demonstration mission, unless a loose and safe formation configuration can be assured), and that the dynamic representation yield time varying models. Most of the

*Corresponding author. Senior Engineer, Simulation & Control Section. Ronda de Poniente 19, Edificio Fiteni VI, Ph: +34-91-806-3462, Email: andres.marcos@deimos-space.com

†Head Simulation & Control Section. Ronda de Poniente 19, Edificio Fiteni VI, Ph: +34-91-806-3473, Email: luis-felipe.penin@deimos-space.com AIAA senior member

‡Project Manager. Av. D.João II, Edificio Torre Zen 8B, Ph: +351-21-893-3018, Email: emanuele.disotto@deimos.com.pt AIAA member

§ESA Project Technical Officer. Keplerlaan 1, Postbus 299, Ph: +31-71-565-6565, Email: remi.drai@esa.int

research has focused up to now in circular FF control[1,2] with the exception of,[3] which initially explored the possibility of using linear parameter varying (LPV) and linear fractional transformation (LFT) techniques for HEO-FF control but finally used LTI gain-scheduled $\mathcal{H}_\infty$ techniques.

In this paper, a HEO-FF relative control design based on nonlinear dynamic inversion (NDI) technology is presented for a three-satellite formation. It is shown that the controller can successfully cope with strong navigation errors, noise, environmental perturbations and uncertainty present through out the experimental phase (and with relatively minor position errors in the rest of the orbit). The layout of the paper is as follows: Section II presents the general FF-GNC architecture proposed while Section III presents the reference mission and state-of-the-art FF engineering simulator used. Section IV covers the selection of the control technology and its application to the FF relative control problem. Sections V and VI show the baseline and Monte-Carlo results, ending with the conclusions in Section VII.

II. Formation Flying Control Architecture

In this section, the proposed FF GNC architecture is presented. This architecture generally sets the FF control problem in terms of the available inputs, outputs and states. A leader-following scheme is used, whereby one vehicle is chosen to be the leader (or target) while the remaining spacecrafts are designated as followers (or fliers), Figure 1 shows a quite generic architecture for this class of schemes. The specific architecture proposed incorporates the Formation Planning & Formation Coordination blocks within the leader SC, which actually is free to drift (has no control or navigation blocks), while the follower SC uses a general input to the guidance block (defined either by the Formation Coordination block or coming from an on-ground operator).

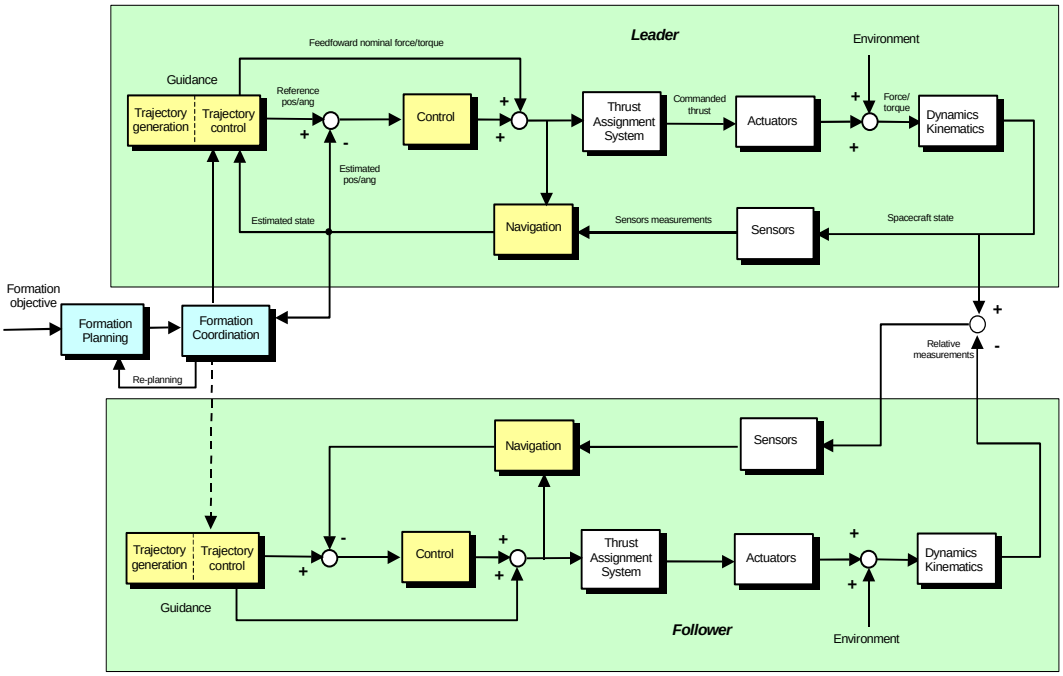

Figure 1. Proposed leader-follower FF GNC architecture.

The navigation function is responsible for estimating the current state of the spacecraft for those variables deemed relevant, besides position/velocity, for guidance and control issues. In FF applications, relative navigation takes much more preponderance than absolute navigation regarding formation manoeuvres and operations. Thus, the FF navigation rationale is approached from a relative navigation point of view (i.e. determination of the relative position/velocity of the satellites within the formation).

The standard suite of navigation components is formed by GNSS systems (applicable only for Earth orbit applications) and, especially prevalent for relative FF navigation, by RF-based, optical and laser methods. The last three methods are used in the specified order following a successive field of view (FOV)

versus accuracy level: RF-based relative navigation is usually employed as a coarse acquisition sensor for formation acquisition at accuracy on the orders of meters. Then, an optical beaconing system would be used as an intermediate acquisition sensor to increase the accuracy to centimetre levels and to provide relative orientation information. Finally, a laser metrology system would be used to provide fine ranging information between spacecrafts.

The SC guidance function is responsible for calculating at each step the reference position/velocity and attitude/attitude-rate to be acquired by the spacecraft. It can be decomposed into two separate functions on each spacecraft: trajectory generation and trajectory control. Their functionality remains as indicated when dealing with only one spacecraft, shown in detail in Figure 2, but new inputs to the trajectory control are required to coordinate between spacecrafts.

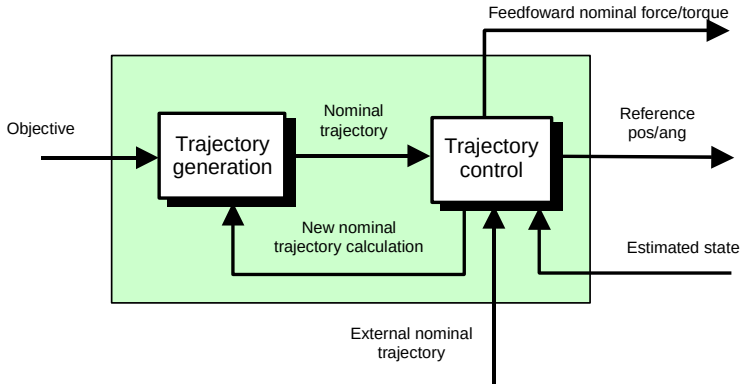

Figure 2. Spacecraft guidance function.

The main difference when considering FF applications is, that the Trajectory Control block can receive as input nominal trajectories coming from the Formation Coordination block instead from its Trajectory Generation function. This is depicted in Figure 2 as an external nominal trajectory input to the spacecraft Trajectory Control block. Important is to remark that when the Formation Coordination or the Trajectory Generation blocks are capable of synthesising a thrust law to achieve a given trajectory in open-loop, this is implemented in the spacecraft as a feed-forward input to the actuators. The guidance rationale consists of generating position references for the FF control block, in line to what should be the desired position of the spacecraft at that instant, based on the nominal reference trajectory input to the Trajectory Control block. This is the most basic type of trajectory control strategy generally applicable, see leader diagram in Figure 1. For tight formation keeping, the nominal trajectory and thus the reference position control will be based on the desired relative distance between spacecrafts.

The SC control function is responsible for generating the actuator commands to be applied to the spacecraft in order to nullify the error in position/velocity or attitude/attitude-rate between the reference value calculated by guidance and the current value calculated by navigation. The term control is used in this article to refer to the function implemented independently on each spacecraft. Indeed, the control system is considered a low level function that directly and continuously generates force/torque commands for the thrust assignment unit implemented in the dedicated set of thrusters. It corresponds to the usual control block in classical control theory.

There is no control function, as it is usually understood, at formation level. At formation level there is the Coordination block that acts as the trajectory control (guidance) function at formation level, calculating reference trajectories for each spacecraft depending on the GNC architecture.

In designing control systems for FF missions, the following factors should be considered:

1. Closed-loop stability and fuel optimality are equally important;

2. The controller cannot be very aggressive (due to the above two requirements) and should not respond to the disturbances that create short-period oscillations;

3. The controller should be capable of preventing any secular growth on long-period oscillations that distort the relative position beyond the tolerance bounds.

4. An additional important point in selecting the control technique, involves the selection of the state and control vectors.

III. Formation Flying Reference Mission

In this section a description of the reference FF mission selected is given together a cursory presentation of the state-of-the-art functional engineering simulator (FES) developed for formation flying studies. The selected orbit is a HEO with a 3,400 Km perigee, a 24 hour period and an eccentricity of 0.768.

This orbit has the great advantage of offering a very quiet environment and of long duration for FF experimentation around apogee (up to 12 hours of experimental time) but on the other hand, it also results in high gravity gradient effects around perigee representing a major FF-GNC design challenge. Indeed, concurrent mission analysis studies show that this orbit location is deemed unsuitable for multiple-SC demonstration missions, unless a loose and safe formation configuration can be assured.

It is assumed that the mass of the S/C is 250kg each and they are shaped as cubes with a side of 1.5 m. The moments of inertia are computed for a uniform distribution of the mass in the cube. Figure 3 shows a pictorial representation of the orbit and the so-called local-vertical-local-horizon (LVLH) reference frame in the formation.

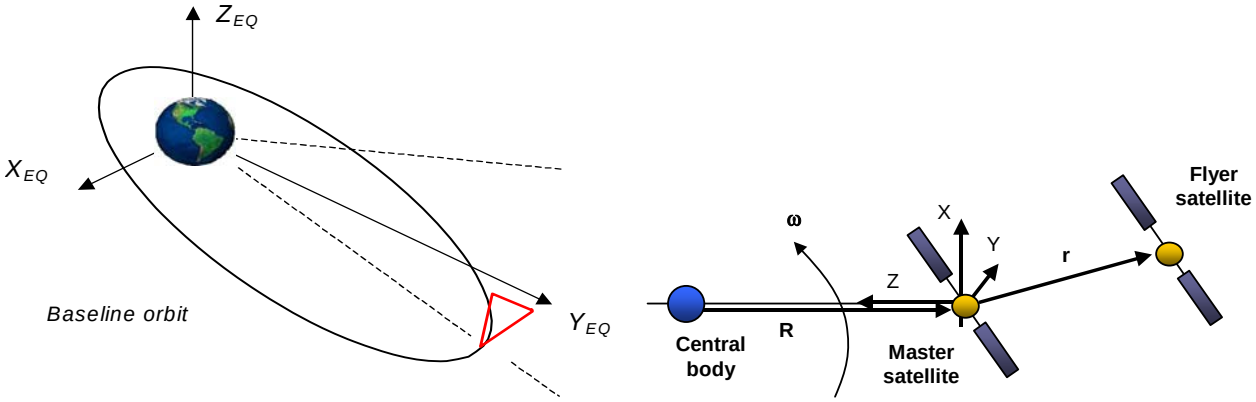

(a) Nominal Orbit. (b) Formation LVLH.

Figure 3. Depiction of the nominal orbit and the three-spacecraft formation in LVLH reference frame.

The LVLH reference frame is the standard coordinate frame used to mathematically model the relative motion of SCs around a central body. It is centred in one of the formation satellites (denoted master or leader), and with respect to which the motion of the rest of the satellites (fliers or followers) is given. Since a great variety of naming conventions are found in the literature regarding the label of each axis, the following convention shall be adopted: Radial relative motions (Z axis) are those in the nadir direction, from the master satellite to the central body. Out-of-plane motions (Y axis) refer to the motions in the opposite direction to that given by the angular motion of the orbit ω, that is, out of the orbital plane of the master satellite; X axis refers to the relative displacements on the in-plane direction that completes the right-hand frame; Table 1 gives the initial relative position of the SCs in the LVLH frame that will be used through out the article (notice that SC2 is in a pure in-plane position while SC3 in an out-of-plane position).

Table 1. Initial relative position and velocity in the LVLH frame.

	Rel. position $[x\ y\ z]$, m			Rel. velocity $[\dot{x}\ \dot{y}\ \dot{z}]$, m/s		
SC 2	-248.17	0	-30.16	0	0	0
SC 3	124.09	-216.5	15.08	0	0	0

Equations of relative motion in a central body gravity field are easily available in the literature, especially in the area of guidance and control for rendezvous and docking operations. They are also usually referred to as differential equations of proximity operations, due to a simplification often performed that considers the distance between master and flier satellites as relatively small compared to the their distance to the central body. A complete derivation of the relative motion dynamics equations can be found in.[4] Equation 1 gives

the final relative motion description of two spacecrafts in the LVLH reference frame:

$$\begin{bmatrix}\ddot{x}\\ \ddot{y}\\ \ddot{z}\end{bmatrix} = \begin{bmatrix}0 & 0 & 2\omega\\ 0 & 0 & 0\\ -2\omega & 0 & 0\end{bmatrix}\begin{bmatrix}\dot{x}\\ \dot{y}\\ \dot{z}\end{bmatrix} + \begin{bmatrix}\omega^2 - k\omega^{3/2} & 0 & \dot{\omega}\\ 0 & -k\omega^{3/2} & 0\\ -\dot{\omega} & 0 & \omega^2 + 2k\omega^{3/2}\end{bmatrix}\begin{bmatrix}x\\ y\\ z\end{bmatrix} + \begin{bmatrix}1 & 0 & 0\\ 0 & 1 & 0\\ 0 & 0 & 1\end{bmatrix}\begin{bmatrix}a_x\\ a_y\\ a_z\end{bmatrix} \quad (1)$$

Where ω is the angular orbital velocity, $\dot{\omega}$ its rate, $k = \mu/h^{1.5}$ is a constant determined by the mean orbital elements, and $a_{x/y/z} = [a_{fp} + a_f - a_{mp} - a_m]_{x/y/z}$ implies total accelerations along each axis (where a_m are the accel. from the master SC's actuators, a_{mp} condenses all the other accel. effects, except gravity, on the master satellite and a_f, a_{fp} are the equivalent accelerations for the fliers satellites). Nevertheless, from now on it is assumed that $a_{x/y/z}$ represent only the thrust acceleration commands along each axis (i.e. $a_{fp} = a_{mp} = 0$).

It is highlighted that the above equation is valid for orbits of any eccentricity (subject to the proximity assumption). For design and analysis purposes, equation (1) can be re-written in a nonlinear state-space formulation using a relative position error $y_e = [x_e\ y_e\ z_e]^\top$, assuming an external reference relative position input vector $u_{ref} = [x_{ref}\ y_{ref}\ z_{ref}]^\top$, and using short-hand notation $\dot{\hat{x}} = [\dot{x}\ \dot{y}\ \dot{z}]^\top$, $\hat{a} = [a_x\ a_y\ a_z]^\top$:

$$\begin{bmatrix}\ddot{x}\\ \ddot{y}\\ \ddot{z}\\ \dot{x}\\ \dot{y}\\ \dot{z}\end{bmatrix} = \begin{bmatrix}0 & 0 & 2\omega & \omega^2 - k\omega^{3/2} & 0 & \dot{\omega}\\ 0 & 0 & 0 & 0 & -k\omega^{3/2} & 0\\ -2\omega & 0 & 0 & -\dot{\omega} & 0 & \omega^2 + 2k\omega^{3/2}\\ 1 & 0 & 0 & 0 & 0 & 0\\ 0 & 1 & 0 & 0 & 0 & 0\\ 0 & 0 & 1 & 0 & 0 & 0\end{bmatrix}\begin{bmatrix}\dot{x}\\ \dot{y}\\ \dot{z}\\ x\\ y\\ z\end{bmatrix} + \begin{bmatrix}1 & 0 & 0\\ 0 & 1 & 0\\ 0 & 0 & 1\\ 0 & 0 & 0\\ 0 & 0 & 0\\ 0 & 0 & 0\end{bmatrix}\begin{bmatrix}a_x\\ a_y\\ a_z\end{bmatrix} \quad (2)$$

$$= \begin{bmatrix}\Gamma_1 & \Gamma_2\\ I_3 & 0_3\end{bmatrix}\begin{bmatrix}\dot{\hat{x}}\\ \hat{x}\end{bmatrix} + \begin{bmatrix}I_3\\ 0_3\end{bmatrix}\begin{bmatrix}\hat{a}\end{bmatrix} \quad (3)$$

$$\begin{bmatrix}\dot{\hat{x}}\\ \hat{x}\\ y_e\end{bmatrix} = \begin{bmatrix}I_3 & 0_3 & 0_3\\ 0_3 & I_3 & 0_3\\ 0_3 & -I_3 & I_3\end{bmatrix}\begin{bmatrix}\dot{\hat{x}}\\ \hat{x}\\ u_{ref}\end{bmatrix} \quad (4)$$

It is important to note, that the FF relative control problem is now transformed into a full state-feedback problem, since the y_e vector is only used as a performance channel. Furthermore, it can be now formally defined as: "design a control system which produces $\hat{a}$ such that the relative error vector y_e formed by subtracting from the reference input vector u_{ref} the navigation estimated relative position $\hat{x}$ tends to zero and such that the resulting closed-loop is stable (asymptotically for all possible perturbations, errors and uncertainties)".

A functional engineering simulator (FES) representing a state-of-the-art software simulation environment has been developed as part of advanced FF studies. It includes independent, but equal, blocks for each spacecraft containing an absolute (inertial) dynamic and kinematic (DKE) model with environmental perturbations, to generate deviations from the theoretical Keplerian motion, and a dynamic propagator based on the formulation given by the Cowell's method. Each spacecraft GNC is formulated using the proposed architecture from Section II, including the navigation suite outlined, and is prepared to accept individual attitude and FF control systems. The perturbation models included in the absolute DKE models are prepared to simulate: J2 and higher order harmonics, third body effects, and solar radiation pressure (SRP) effects. Similarly, the SC GNC models contain navigation errors and noise together uncertainty models for the system parameters and input/output channels (more about these in Section VI-A).

IV. Formation Flying Control Design

A. FF Control Problem Evaluation

In the previous section a formulation of the relative motion of two spacecrafts moving in an highly eccentric orbit and measured in a LVLH reference frame with origin in the target spacecraft, equations (1-4), was given. Based on these equations and the selected HEO orbit, the following characteristics can be observed:

1. The relative motion is highly (e.g. drastic changes from apogee to perigee) time-varying (e.g. dependent on ω and $\dot{\omega}$) and nonlinear (e.g. ω^2 and $\omega^{3/2}$ terms).

2. The states and control inputs enter the system in a very clear and linear manner.

3. The dynamics are relatively slow.

4. The system is Multi-Input-Multi-Output (MIMO) but it is well decoupled into in-plane motion (X-Z plane) and out-of-plane motion (Y-plane). Thus, it can be consider as a stacked system formed by two independent systems: a 2 input/output MIMO and a SISO system.

5. The uncertainty arises from the inexact knowledge/estimation on ω, $\dot{\omega}$ and on the relative position/velocity state vectors; while the perturbations enter the system linearly, through the acceleration vector (now expanded to the original form) $a_{x/y/z} = [a_{fp} + a_f - a_{mp} - a_m]_{x/y/z}$.

In addition to the above characteristics, it is desired to perform a proof-of-concept control design to assess the feasibility of developing a control law for the complete orbit (including formation acquisition, experimental phase requirements and perigee passage formation control).

Assessing all the above characteristics from a modern control perspective, the most potential-looking candidate techniques are: linear parameter varying (LPV) and nonlinear dynamic inversion (NDI). The former is somewhat more involved and typically result in control designs with larger number of states, although for highly time-varying/nonlinear MIMO systems it provides a control design process with explicit robustness characteristics. The latter provides a very straightforward theoretical and easy to implement control approach but might suffer of robustness problems.

In the present case, due to the very slow dynamics involved in the motion, it is expected that the NDI approach might be the most straight forward candidate technique for a proof-of-concept design. Furthermore, in case its robustness characteristics need to be explicitly augmented, techniques forming the background theory of the LPV approach (such as $\mathcal{H}_\infty$-optimization, μ-design or even LPV) can be used without major modifications to the control loop. Thus, NDI is the selected candidate control technique in the present article.

B. NDI design

NDI is a promising technology widely used in aircraft but that only recently has started being considered for space applications.[5–7] It can be summarized as a three main step process, see Figure 4: definition of the controlled variable (CV), characterization of the desired dynamics and inversion of the dynamics. The objective is to achieve the desired response for the CV vector x to command vector x_c, i.e. to drive the error vector x_e to zero (x_p in the figure refers to the feedback vector).[8]

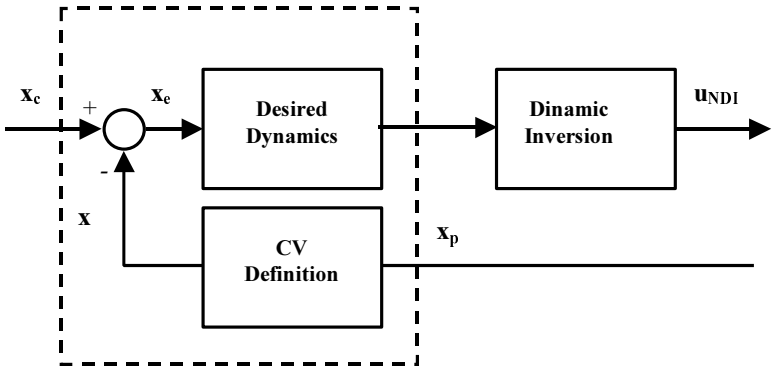

Figure 4. FF-NDI control architecture.

For the relative FF problem, the controlled variable definition consists of transforming the line-of-sight (LOS) and distance measurements into relative position and velocity vectors. Then, the desired dynamics are specified paralleling a standard ideal second-order representation. Finally, the dynamic inversion is performed and consists of two sub-steps: one the proper inversion of the dynamics and second, a control allocation scheme (typically, used when there are more control effectors than control variables).

In this article, we will focus only in the first two main steps: CV definition and desired dynamic achievement, since a main assumption is that the control distribution matrix is an identity. As the study was developed for a technological proof-of-concept this assumption suffices, but it is recognized that the subsequent step will be to implement realistic actuator models with magnitude limitations and invert the associated control effector distribution matrix and firing time limits (although there is already a simplex thrust allocation method implemented and used in the FES).

It is straightforward to derive the NDI control input $u_{NDI} = [a_x\ a_y\ a_z]^\top$ from the short-hand version of the relative motion equations:

$$\left[u_{NDI}\right] = -\begin{bmatrix}\Gamma_1 & \Gamma_2\end{bmatrix}\begin{bmatrix}\dot{\hat{x}}\\ \hat{x}\end{bmatrix} + \left[\ddot{\hat{x}}\right]_{des} \tag{5}$$

Now, the question is how to obtain the desired vector $\ddot{\hat{x}}_{des}$, which represents the new desired commands. A classical control approach using a 2nd order reference model is followed (see[9] for an example of this approach to aircraft control).

First, note that although this is a second-order differentiation on the relative position vector this just means that a double integrator is needed between the desired commands and the measured relative position vector. This can be represented as follows, where PID_1, PID_2 indicate standard proportional-integral-derivative control design:

$$\left[\ddot{\hat{x}}\right] = PID_1\left(\left[\dot{\hat{x}}\right]_{des} - \left[\dot{\hat{x}}\right]_{meas}\right) = PID_1\left(PID_2\left(\left[\hat{x}\right]_{ref} - \left[\hat{x}\right]_{meas}\right) - \left[\dot{\hat{x}}\right]_{meas}\right) \tag{6}$$

Now, note that rather than designing two sequential PID blocks, one for the relative position error and the other for the relative velocity error, it is possible to simplify the design process conceptually as follows:

$$\left[\ddot{\hat{x}}\right] = \Pi_1\left(\left[\hat{x}\right]_{ref} - \left[\hat{x}\right]_{meas}\right) - \Pi_2\left[\dot{\hat{x}}\right]_{meas} \tag{7}$$

Taking Laplace transforms (assuming zero initial conditions) and re-arranging yields:

$$\ddot{\hat{x}}_m = \Pi_1\hat{x}_{ref} - \Pi_1\hat{x}_m - \Pi_2\dot{\hat{x}}_{ref} \quad \Rightarrow \quad \hat{x}_m = \frac{\Pi_1}{s^2 + \Pi_2 s + \Pi_1}\hat{x}_{ref} \tag{8}$$

Thus, by equivalence to the standard 2nd order model $x = \omega^2/(s^2 + 2\zeta\omega s + \omega^2)$ the following relations are obtained (repeated for each axis):

$$\Pi_{1-x} = \omega_x^2 \qquad \Pi_{2-x} = 2\zeta_x\omega_x \tag{9}$$

The gain selection for each of the axis is further simplified recalling that the relative motion is essentially decoupled (i.e., it is fully decoupled from the relative perspective but not from the absolute point of view) into in-plane (X-Z plane) and out-of-plane (Y-axis) motions. Thus, by first tuning the out-of-plane motion and subsequently the in-plane motion it is fairly easy to arrive to a good design. For the present case, it sufficed a few iterations to arrive at the selected gains, given in Table 2.

Table 2. FF-NDI controller gains.

	$\Pi_1 = K_P = \omega^2$	$\Pi_2 = K_D = 2\zeta\omega$	$K_I = \alpha$
X-axis	0.02^2	$2 \cdot 2 \cdot 0.02$	$8e^{-6}$
Y-axis	0.04^2	$2 \cdot 1 \cdot 0.04$	$5e^{-6}$
Z-axis	0.02^2	$2 \cdot 2 \cdot 0.02$	$6e^{-6}$

As seen in the table, it was necessary to incorporate an integral gain for the position error to eliminate residual steady-state offsets. It was decided to add integral action in such a manner that these small errors could be removed but that we still had the conceptual 2nd order approach shown before. This was done by selecting an integral gain much smaller than the proportional gain so as to be considered negligible conceptually:

$$\ddot{\hat{x}}_m = \left(\Pi_1 + \frac{\alpha}{s}\right)(\hat{x}_{ref} - \hat{x}_m) - \Pi_2 \dot{\hat{x}}_{ref} \quad \Rightarrow \quad \hat{x}_m = \frac{\tilde{\Pi}_1}{s^2 + \Pi_2 s + \tilde{\Pi}_1} \hat{x}_{ref} \tag{10}$$

$$\tilde{\Pi}_1 = \Pi_1 \left(1 + \frac{\alpha \backslash \Pi_1}{s}\right) \quad \text{such that} \quad \frac{\alpha}{\Pi_1} << 1 \tag{11}$$

Combining the above equations the complete NDI FF relative-motion control is obtained.

V. Baseline Analysis

In this section two types of analyses are performed: one for the open-loop (OPL) and the other for the closed-loop (CLP). These analyses establish the baseline comparison and provide an understanding into the physical problem (i.e. the mechanics and dynamics involved).

The baseline simulation starts close to the apogee after the three satellites have been released from the launcher, have been de-tumbled and relative velocity between the SCs has been reduced, i.e. the relative positions/velocities among the satellites were given in Table 1. No perturbations (except for a J2 gravitometric model), nor errors or uncertainties are used in these baseline simulations.

A. Open loop analysis

Figure 5 shows the absolute relative error of the follower satellites (SC 2 and 3) with respect to the master satellite in the relative target-frame (LVLH). It is clear from the figure that the relative position errors of the satellites when no FF-NDI control is used are quite large in all the axes (and for both satellites, each completely independent of each other except that both follow SC 1). Furthermore, although no infinitely large instability (departure) occurs in the time responses, it is observed that the large errors obtained and their continuous increment with time indicates a probable open-loop instability (ascertained next using open-loop frozen-time eigenvalue analysis).

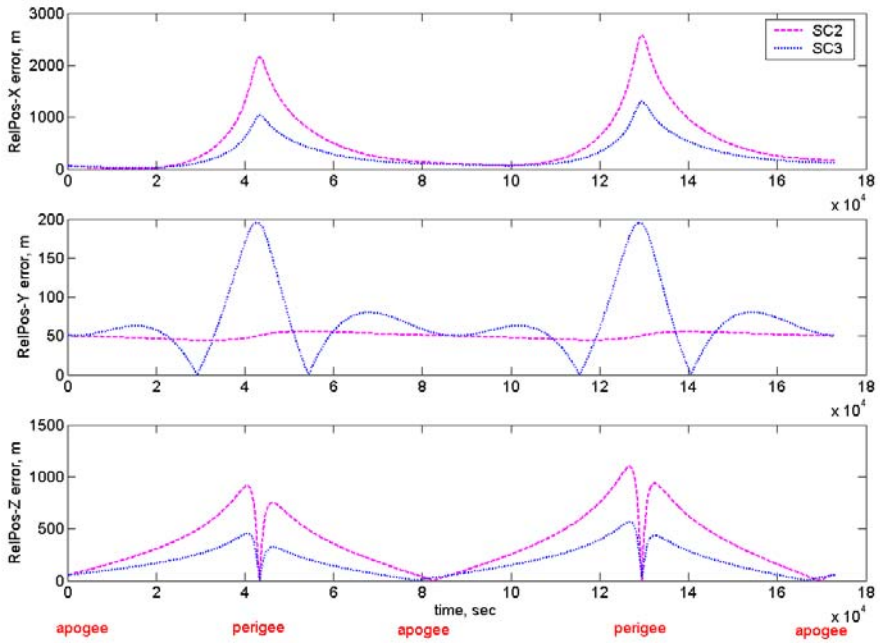

Figure 5. OPL baseline: relative motion w.r.t. SC1 in LVLH frame.

Using the state matrix from the system equation (4) together the above open-loop orbits (from where the orbital rate and acceleration are obtained), an OPL frozen-time eigenvalue analysis is performed along the trajectory, see Figure 6. In the figure, the rectangles indicate the range of the eigenvalues. As it was

observed before in the time simulation, the OPL system is unstable and this instability increases with time (it is recalled and highlighted again that these OPL simulations are performed without any environmental perturbation or noise except for the J2-gravity perturbation). Note that the level of instability is small, the eigenvalues are all between ± 0.0005. These OPL results are in agreement with previous studies.[3,4]

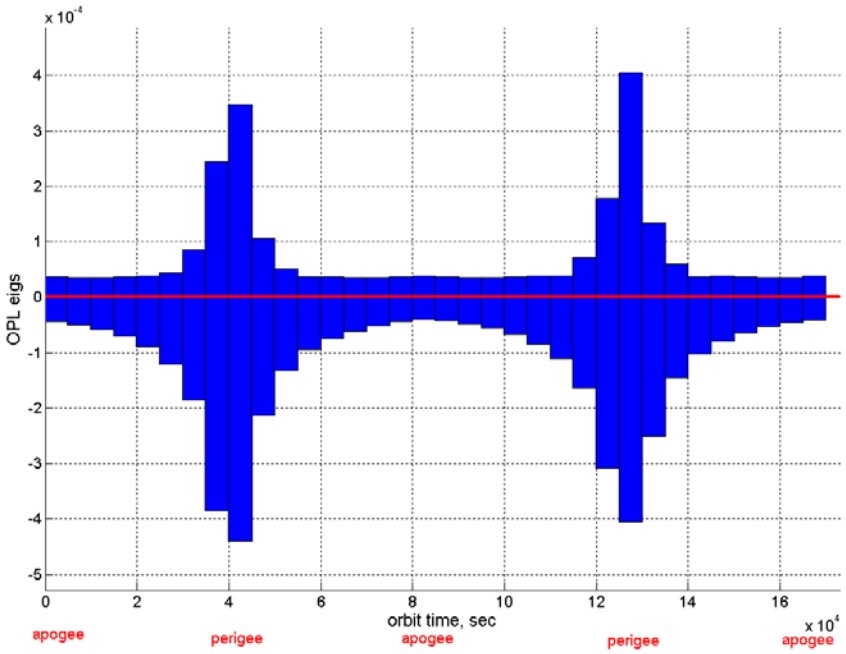

Figure 6. OPL baseline: frozen-time eigenvalue analysis for SC2.

B. Closed loop analysis

Once the behaviour of the un-controlled formation has been ascertained, the capability of the designed NDI FF relative-motion controller is assessed under the same simulation environment.

In order to evaluate the capability (if ever needed) for the FF-controller to perform formation acquisition tasks and to better judge its temporal characteristics (overshoot, rise time, etc), a reference input u_{ref} is used for each of the follower satellites, see Table 3. It is highlighted that this is a task typically performed by the FF-guidance system (which is not-active in the present case since constant references are used as inputs to the FF-control function).

Table 3. Commanded relative position u_{ref} in the LVLH frame, m.

SC 2	-50	50	-50
SC 3	50	50	50

Figure 7 shows the CLP absolute errors for all axes. Due to the large initial closed-loop reference command used, the time responses are divided in three sections: the left-most plots consider the first 5000 seconds of the simulation (to showcase the rise-time and overshoot characteristics), the center column which shows the rest of the responses and the right-most plots zooms-in into the rectangle area shown in the center column corresponding to an apogee experimentation phase. It is observed that the maximum errors achieved by the NDI FF-controller are respectively for each axis [0.4 0.3 0.4] meters and moreover, these errors are achieved during perigee passage –not counting the initial errors of course. For the experimental phase around the apogee, the errors are in the order of ±0.02 meters for all axes. This indicates a very successful accomplishment in keeping the formation tight during the experiment-observation phase and even during the fast-dynamical environment around the perigee -when facing only J2 perturbations.

Figure 8 shows the corresponding thrust forces (which can be used as an indicator of the fuel consumption)

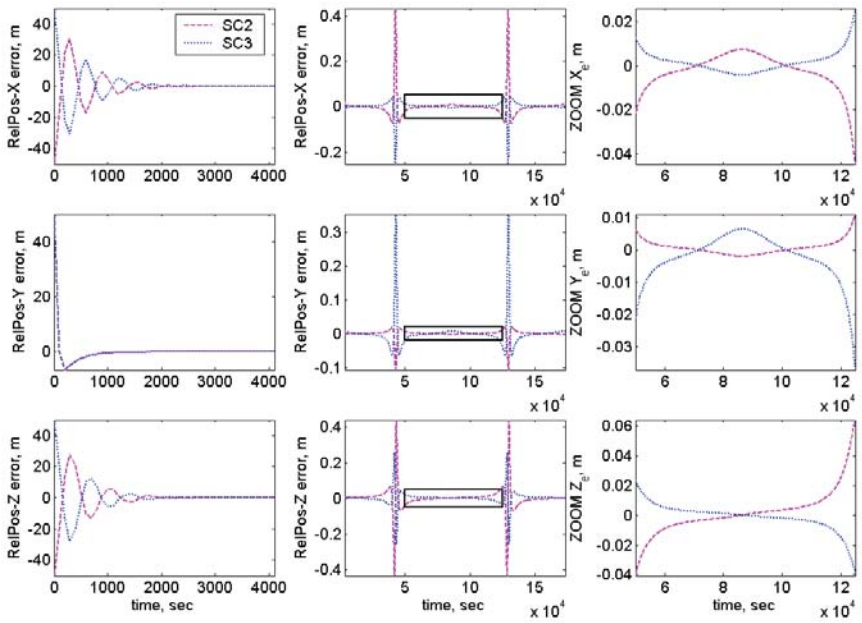

Figure 7. CLP baseline: relative motion w.r.t. SC1 in LVLH frame.

for the equivalent period of time as in the previous figure's center and right-most columns. It is observed that a very small consumption, with peaks around the perigee of magnitude smaller than 0.05N, is demanded by the NDI controller, which can be considered adequate for this type of missions when using cold gas low thrusters.

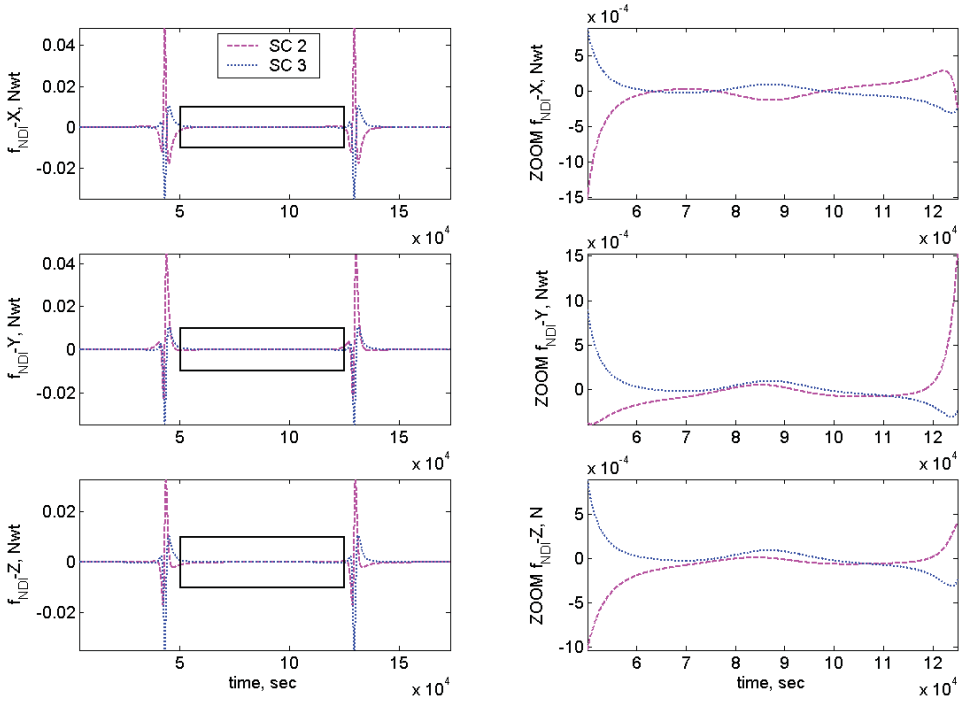

Figure 8. CLP baseline: commanded forces ($f = a \cdot mass$) for SC2 & SC3.

VI. Closed Loop Monte Carlo Analysis

In order to assess the robustness of the NDI-FF-control design, a preliminary Monte-Carlo (MC) analysis is performed using random variations on the state-feedback controller input vector (the relative position $\hat{x}$ and velocity $\dot{\hat{x}}$ vectors), on the system parameters used by the NDI controller (ω and $\dot{\omega}$) and also on the orbital perturbations.

A. Perturbations, noise, errors and uncertainties

A differentiation is made between perturbations (e.g. environmental changes such as those arising from J2-gravitational effects or atmospheric drag), noise, navigation LOS errors and system parameters' uncertainty. All the Monte-Carlo random parameters are generated at the beginning of each Monte-carlo shot, each with different seeds so that the random generators in charge of varying their values are uncorrelated.

For the system (ω and $\dot{\omega}$) parameters' uncertainty, a multiplicative model with normalized random parameter ν is used: $\omega_{est} = \omega(1 + \Delta_\omega \nu)$, where $\Delta_\omega = 0.3$ and ν is obtained randomly from a Gaussian distribution with 0 mean and variance 1. Therefore, the above multiplicative model represents a very conservative level of uncertainty, up to $\pm$ 30 percent on the orbit determination system parameter.

Navigation line-of-sight (LOS) errors for the relative position $\hat{x}$ and velocity vectors $\dot{\hat{x}}$ are also implemented. This is more complex than above as it is required to take into account four different source of errors: relative distance error δ_D, relative speed error $\delta_{\dot{D}}$, line-of-sight error δ_{LOS} and also line-of-sight rate error $\delta_{L\dot{O}S}$. Quite conservative values are used also for these four relative navigation errors, see Table 4:

Table 4. Navigation sensor performance errors.

	LOS	**Distance**
position	$\delta_{LOS} < 1$ deg	$\delta_D < 0.01$ m
rate	$\delta_{L\dot{O}S} < 0.1$ deg/sec	$\delta_{\dot{D}} < 0.001$ m/s

When calculating the navigation LOS errors there are two different angles that need to be considered (one rotating along the X-axis and the other along the Y-axis, always in the LVLH frame). These two LOS angle perturbations can be assumed projected into angle perturbations on spherical coordinates errors: δ_α, $\delta_{\dot{\alpha}}$ and δ_β, $\delta_{\dot{\beta}}$ as shown in Figure 9. Similarly, the distance errors, δ_D and $\delta_{\dot{D}}$, can be assumed projected on distance spherical coordinate errors, δ_r and $\delta_{\dot{r}}$.

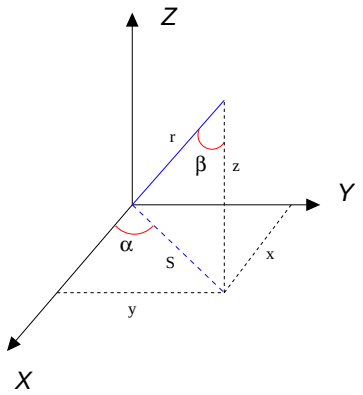

Figure 9. Navigation error projection.

Using the standard transformation from spherical to Cartesian coordinates (i.e. the desired LVLH frame) and assuming a fixed (but randomly calculated at the beginning of each Monte-Carlo shot) value for the spherical errors (δ_α, $\delta_{\dot{\alpha}}$, δ_β, $\delta_{\dot{\beta}}$, δ_r and $\delta_{\dot{r}}$) the error-corrected estimated relative position and velocity vectors are obtained. It is noted that errors of up to $\pm$ 4 meters and $\pm$ 0.002 m/s are obtained for the relative position and velocity vectors respectively (these are extremely high errors more typical of a coarse RF navigation than of the typical laser-based sensors used in tight formation control).

Once the error-influenced relative position $\tilde{x}$ and velocity vectors $\dot{\tilde{x}}$ are obtained, each component is further perturbed by noise σ (using again uncorrelated random generators for each component). The magnitude of the noise is $\pm$ 1 percent of the relative vector variation $x_{est} = \tilde{x} + (\tilde{x} - x)0.01\sigma$.

In the subsequent analysis, it is shown these errors are indeed quite drastic driving the main performance objectives (i.e. small relative position errors and small fuel consumption) to the limits, but acceptable.

B. Results

Finally, the MC results using the above errors, uncertainties and perturbations are presented. The same LVLH initial satellite position and velocity vectors as those in given in Table 1 are used (the reference input vector u_{ref} is now the initial vectors from that table). Due to the random number generation at each shot initialization, the initial position vectors are a little off with respect to those commanded.

A total of 500 runs are used (each run takes about 10 minutes on a 3MHz Pentium pc with 1Gb Ram using a sample-time of 10 seconds). Notice that since there are two flier-satellites in the formation (each completely independent of the other in terms of dynamic propagator, perturbations, noise, etc), it implies that there are 1000 independent runs and thus a reliable statistical analysis can be performed.

Figure 10 shows the absolute relative position errors of both flier-satellites (in the left column) and the corresponding demanded thrust (right column) for the time segment simulated for this MonteCarlo analysis (half that used in Figures 5 $\rightarrow$ 8). This time segment starts close to the apogee and ends after one period, a total of 23.6 hours, and represents a combined experimental phase of approximately 8 hours –from 5,000 to 20,000 secs plus from 70,000 to 86,000 seconds. Figure 11 zooms in the second part of the experimental phase $[70,000 - 86,000]$ seconds, to allow better visualizing the performance of the FF-controller during the typically most important phase on an orbit, that of experimentation around the apogee. Both figures present only the first 25 MonteCarlo runs due to the otherwise large size of the figures.

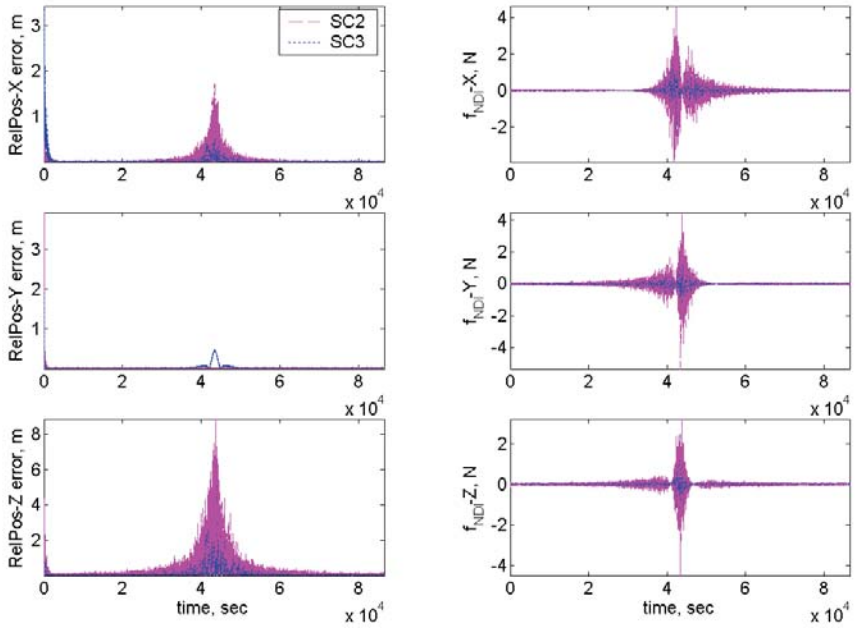

Figure 10. MC analysis: relative motion w.r.t. SC1 in LVLH frame.

In figure 10 it is observed that the maximum relative position errors for each axis are respectively [2 0.1 8] meters approximately while the maximum thrusts demanded by the FF-controller vary between $\pm$4 Newtons, but note that these maximum errors are always around the perigee where the dynamics are most aggressively changing. Similar to previous figures, the initial error introduced at the beginning of simulation is completely absorbed by the controller after 4000 seconds with thrust commands of similar value to those in the experimental phase (it is noted that this initial position errors are around [3 4 5] meters).

In order to assess better the performance of the FF-controller around the apogee, Figure 11 shows the above time responses but focusing on the second experimental phase (after the perigee). It is appreciated

that the relative position errors for the X and Y axes are below 0.05 meters while for the Z-axis below 0.25 meters. Similarly, the demanded thrusts are all ± 0.07 Newtons (slighlty above the ± 0.05 N limit but nevertheless quite good due to the drastic levels of noise and uncertainty assumed). Additionally, it is highlighted that the control objective was to minimize thrust and position error for the entire orbit (i.e. formation acquisition, apogee and perigee), if as it is more usual, a FF-controller were to be designed for the experimentation phase alone the gains given in Table 2 will be changed to satisfy the more stringent position error and thrust commands required for tight formation keeping during this phase.

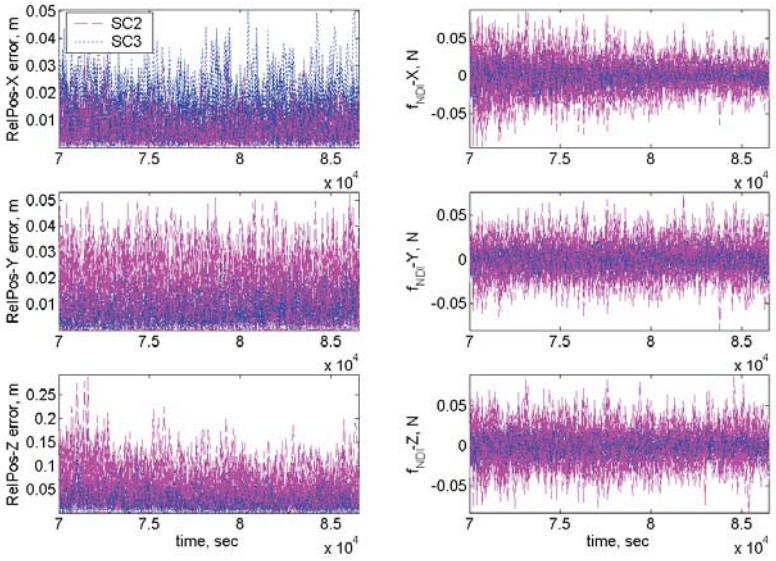

Figure 11. MC analysis: thrust consumption for SC2 & SC3.

In order to appreciate the conservative level used for the uncertainty and noise variations, Figure 12 shows the perturbed inputs fed to satellite 2 controller by the navigation function. The left column shows the relative position estimates and it is observed the variations are quite spread among the Monte Carlo runs, indicating that the controller can react well to large errors. Similarly, the right column shows the relative velocity vector used, which ideally should be close to zero.

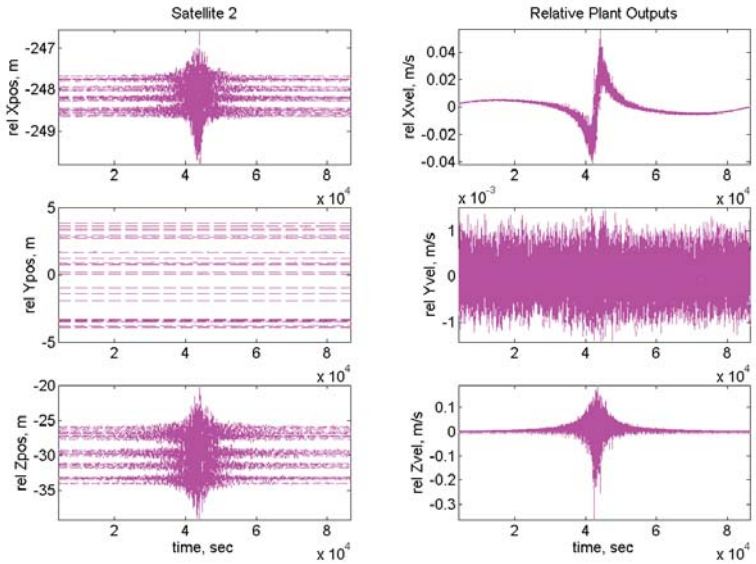

Figure 12. MC analysis: perturbed controller input vector for SC2.

Finally, using the combined (from both satellites) 1000 time responses, Table 5 shows the main statistical values for the MonteCarlo analysis for the second experimentation phase, i.e. $t = [70,000 - 86,000]$ seconds: mean, standard deviation (std) and maximum for the relative position errors and demanded thrusts along each axis. Note that the mean of the demanded (absolute module) thrust is well within the limits.

Table 5. Monte Carlo statistical analysis (1000 runs).

	$\mathbf{X_{error}}$	$\mathbf{Y_{error}}$	$\mathbf{Z_{error}}$	$\mathbf{X_{thrust}}$	$\mathbf{Y_{thrust}}$	$\mathbf{Z_{thrust}}$
mean	0.009 m	0.009 m	0.040 m	0.011 N	0.015 N	0.014 N
stad	0.006 m	0.006 m	0.031 m	0.010 N	0.012 N	0.012 N
max	0.066 m	0.042 m	0.194 m	0.116 N	0.138 N	0.117 N

VII. Conclusion

In this article, an evaluation and preliminary design of a modern control technique for non-circular orbit formation flying control has been presented. The purpose was to evaluate if there was a candidate control technique valid for the complete orbit, including formation acquisition task, apogee and perigee passages. The control technique selected is based on nonlinear dynamic inversion, a promising technology widely used in aircraft but that only recently has started being considered for space applications. It has been shown in preliminary analyses that the controller performs quite well during the experimental phase even in the face of very conservative errors and system uncertainty values, and that during the more demanding perigee passage it still had relatively acceptable performance.

Acknowledgments

This research was supported by ESA / ESTEC Contract number 19495/04/NL/JA/pg.

References

[1]Kapila, V., Sparks, A., Buffington, J., and Yan, Q., "Spacecraft Formation Flying: Dynamics and Control," *Journal of Guidance, Control, and Dynamics*, Vol. 23, No. 3, May-June 2000, pp. 561–564.

[2]Kang, W., Sparks, A., and Banda, S., "Coordinated Control of Multisatellite Systems," *Journal of Guidance, Control, and Dynamics*, Vol. 24, No. 2, March-April 2001, pp. 360–368.

[3]Gaulocher, S., Chrétien, J.P., Pittet, C., Delpech, M., and Alazard, D., "Closed-Loop Control of Formation Flying Satellites: Time and Parameter Varying Framework," *2nd International Symposium on Formation Flying Missions & technologies*, Washington D.C., USA, September 2004.

[4]Yamanaka, K. and Ankersen, F., "New State Transition Matrix for Relative Motion on an Arbitrary Elliptical Orbit," *Journal of Guidance, Control, and Dynamics*, Vol. 25, No. 1, January-February 2002, pp. 60–66.

[5]Juliana, S., Chu, Q.P., Mulder, J.A., and van Baten, T.J., "Nonlinear Flight Control for Re-Entry Flight Vehicle," *55th International Astronautical Congress*, Vancouver, CA, 2004.

[6]Da Costa, R.R., Chu, Q.P., and Mulder, J.A., "Re-entry Flight Controller Design Using Nonlinear Dynamic Inversion," *Journal of Spacecraft and Rockets*, Vol. 40, No. 1, 2003.

[7]Marcos, A., Peñín, L.F., Caramagno, A., Sommer, J., Belau, W., and Bornschlegel, E., "Design of a fully automated NDI attitude controller for the Hopper atmospheric re-entry," *17th Conference on Automatic Control in Aerospace*, Toulouse, FR, June 2007.

[8]Enns, D., Bugajski, D., Hendrick, R., and Stein, G., "Dynamic Inversion: an evolving methodology for flight control design," *International Journal of Control*, Vol. 59, No. 1, 1994, pp. 71–91.

[9]Bennani, S. and Looye, G., "Flight Control Law Design for a Civil Aircraft using Robust Dynamic Inversion," *IEEE/SMC-CESA 98 Congress*, Tunisia, April 1998.